JGR Atmospheres

RESEARCH ARTICLE
10.1029/2018JD030085

The Impact of Human-Induced Climate Change on Regional Drought in the Horn of Africa

T. R. Marthews[1], R. G. Jones[2,3], S. J. Dadson[1,2], F. E. L. Otto[4], D. Mitchell[5], B. P. Guillod[6,7], and M. R. Allen[4]

[1]Centre for Ecology and Hydrology, Wallingford, UK, [2]School of Geography and the Environment, University of Oxford, Oxford, UK, [3]Met. Office Hadley Centre, Met. Office, Exeter, UK, [4]Environmental Change Institute, University of Oxford, Oxford, UK, [5]School of Geographical Sciences, University of Bristol, Bristol, UK, [6]Institute for Environmental Decisions, ETH Zurich, Zurich, Switzerland, [7]Institute for Atmospheric and Climate Science, ETH Zurich, Zurich, Switzerland

Key Points:
- Precipitation patterns are known to be changing across the Horn of Africa, but trajectories in land surface variables are less well known
- We identify two distinct "drought trajectories" in the Horn of Africa: one of increasing drought and one of decreasing drought
- Changes in water cycle impacts may best be assessed through attribution studies that include changes in land surface variables

Supporting Information:
- Supporting Information S1

Correspondence to:
T. R. Marthews,
tobmar@ceh.ac.uk

Citation:
Marthews, T. R., Jones, R. G., Dadson, S. J., Otto, F. E. L., Mitchell, D., Guillod, B. P., & Allen, M. R. (2019). The impact of human-induced climate change on regional drought in the Horn of Africa. *Journal of Geophysical Research: Atmospheres*, *124*, 4549–4566. https://doi.org/10.1029/2018JD030085

Received 3 DEC 2018
Accepted 2 APR 2019
Accepted article online 8 APR 2019
Published online 30 APR 2019

Author Contributions:
Conceptualization: T. R. Marthews, R. G. Jones, S. J. Dadson, F. E. L. Otto, M. R. Allen
Data curation: F. E. L. Otto
Formal analysis: T. R. Marthews, B. P. Guillod
Funding acquisition: M. R. Allen
Investigation: T. R. Marthews
Methodology: T. R. Marthews, S. J. Dadson
Project administration: M. R. Allen
Resources: T. R. Marthews, F. E. L. Otto
Software: T. R. Marthews
Supervision: S. J. Dadson, M. R. Allen
(continued)

Abstract A severe drought hit the Greater Horn of Africa (GHA) in 2014, but it remains unclear whether this extreme event was attributable to anthropogenic climate change or part of longer-term natural cycles. Precipitation patterns are known to be changing across the GHA, but trajectories in land surface variables are much less well known. We simulated the GHA land surface environment to assess the balance between natural cycles and human-induced climate change. Using a new form of event attribution study where we focused on both climate variables and also directly simulated land surface variables, we combined publicly volunteered distributed computing with land surface simulations to quantify land surface responses. Uncertainty was quantified both for climate model and land surface model outputs. We identified two distinct "drought trajectories" in the GHA bimodal seasonality area during the March–May (Long Rains season) of 2014. Human-induced climate change may have resulted in regions from Lake Nalubaale (Lake Victoria) to Northern Kenya receiving less precipitation in this season and having up to 20% higher probability of drought-level evapotranspiration rates (increasing drought). In contrast, the simulated anthropogenic climate change signal for this season induced somewhat wetter conditions and up to 20% lower probability of drought-level evapotranspiration in Eastern Ethiopia, Southern Somalia, and coastal Kenya (decreasing drought). Uncertainties in our modeling system varied by region and variable of focus, but broadly we found that land surface simulation uncertainty neither added significantly to climate model uncertainty nor significantly reduced it.

1. Introduction

Extreme events such as large-scale droughts are of key global importance (von Buttlar et al., 2017), as is our need to build society's resilience to the consequences and impacts of these events. Drought is primarily associated with precipitation deficit, which can lead to increasing temperatures and decreasing soil moisture. However, drought is not always initiated by low precipitation: Other factors such as radiation, temperature, and cloudiness may also affect evaporation regimes (Dai, 2013; Gregory et al., 1997; Seneviratne et al., 2010; Taylor et al., 2012; Teuling et al., 2009; Teuling et al., 2013). In order to understand the complete dynamical system, it is necessary to look at how climate signals translate into land surface impacts, which necessarily involves taking account of hydrological and land surface factors such as topography, soil moisture, and vegetation cover (Seneviratne et al., 2010).

The Greater Horn of Africa (GHA) is a climatically diverse region covering an area equal to almost half the United States of America. We focus on the area that experiences an annual bimodal rainfall regime (bimodal seasonality area, BSA; Figure 1): the *Long Rains* during March–May as the tropical rain belt crosses the Equator from south to north and the *Short Rains* during October–December as the rain belt returns to the south (Marthews et al., 2015; Nicholson, 2018; Rowell et al., 2015). The long rains in particular have received much recent attention in order to identify the large-scale climate drivers that affect them (Funk et al., 2014; Lyon & DeWitt, 2012; Yang et al., 2014). Dominant drivers include the annual movement of the tropical rain belt across the Equator (also known as the intertropical convergence zone), sea surface temperatures (SSTs) in the Indian Ocean (as indexed, e.g., by the Indian Ocean dipole, IOD) and the degree of coupling between the land surface and the atmosphere in this region (Bierkens, 2015).

An issue of great current concern in the Horn of Africa is the long-term decrease in the precipitation brought by the long rains since 1999 (Lyon, 2014; Lyon & DeWitt, 2012; Nicholson, 2017; Rowell et al., 2015). The

Validation: T. R. Marthews
Visualization: T. R. Marthews
Writing - original draft: T. R. Marthews
Writing – review & editing: T. R. Marthews, R. G. Jones, S. J. Dadson, B. P. Guillod

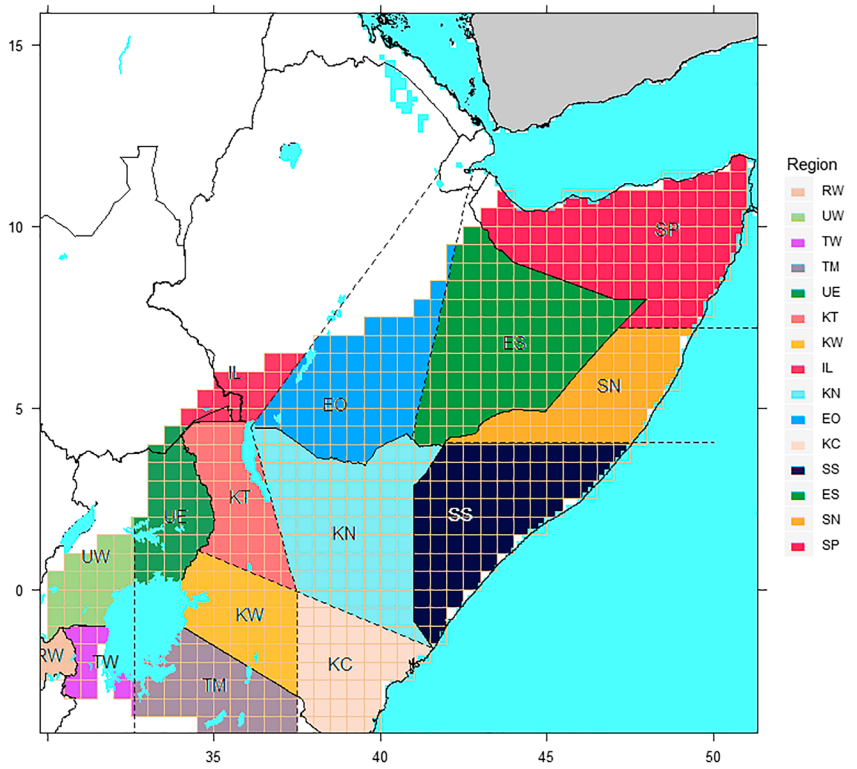

Figure 1. The bimodal seasonality area of the Greater Horn of Africa (gridded), defined as the contiguous area that experienced a Long Rains season (March–May) and a Short Rains (October–December) in most, if not all, years 1983–2012 (TAMSAT data, Tarnavsky et al., 2014; n.b. other zones do have bimodal rainfall patterns—e.g., N. Ethiopia—but are not included because they are separated from the zone shown by consistently unimodal or trimodal zones). The bimodal seasonality area was covered for analysis by a mesh of 0.5° × 0.5° gridcells (n = 655 gridcells), with results from individual gridcells then averaged over more easily-identifiable larger regions for display purposes (colored). The larger regions were selected so as to average approximately 150,000 km^2 and conform to recognizable political and topographical units within the subcontinent. Larger areas shown: SP = Somalia (Puntland and Somaliland); SN = Somalia north of Mogadishu and south of Puntland; SS = Southern Somalia (Mogadishu and south); EO = Ethiopia/Oromia; ES = Ethiopia/Somali; IL = the Ilemi Triangle in South Sudan and Ethiopia/South Omo; KN = Kenya north of a line from Kolbio to Kitale and east of a line from Mt Kenya to Lake Turkana; KT = Kenya north of a line from Kolbio to Kitale and west of a line from Mt Kenya to Lake Turkana; KW = Kenya south and west of Mt Kenya; KC = Kenya from Mt Kenya south and east to the coast; UW = Uganda West of Kampala (western half of Lake Victoria/Nalubaale); UE = Uganda East of Kampala (eastern half of Lake Victoria); TW = Tanzania West of Mwanza (western half of Lake Victoria); TM = Mid-Tanzania from Mt Kilimanjaro westward.

decrease of the long rains has been the dominant driver of the increased frequency and severity of droughts in the GHA in recent years (Boulter et al., 2013; Masih et al., 2014; Yang et al., 2015). Simple regression statistics show that in the GHA evapotranspiration, a simple drought measure (Seneviratne et al., 2010; Teuling et al., 2013) was closely related to precipitation (Figures 2 and 3) during the 2014 Long Rains (Figure 4). In the GHA, models that adequately characterize the long rains within the climate system are the key to greater understanding of the dynamics of major droughts (Yang & Huntingford, 2018). These models are additionally important because they form the basis of drought detection and early warning systems for the subcontinent.

1.1. Climate Event Attribution

General changes in global climate are modifying the frequency of many regional and local events, both in terms of climate and climate impacts (IPCC, 2014; Trenberth, 2012), but how much of this is attributable to human actions and how much is simply interannual variability? It is very challenging to firmly and quantitatively demonstrate a robust anthropogenic effect on extreme events, especially because events such as drought usually occur as a result of a combination of factors (Trenberth et al., 2015). Attribution studies

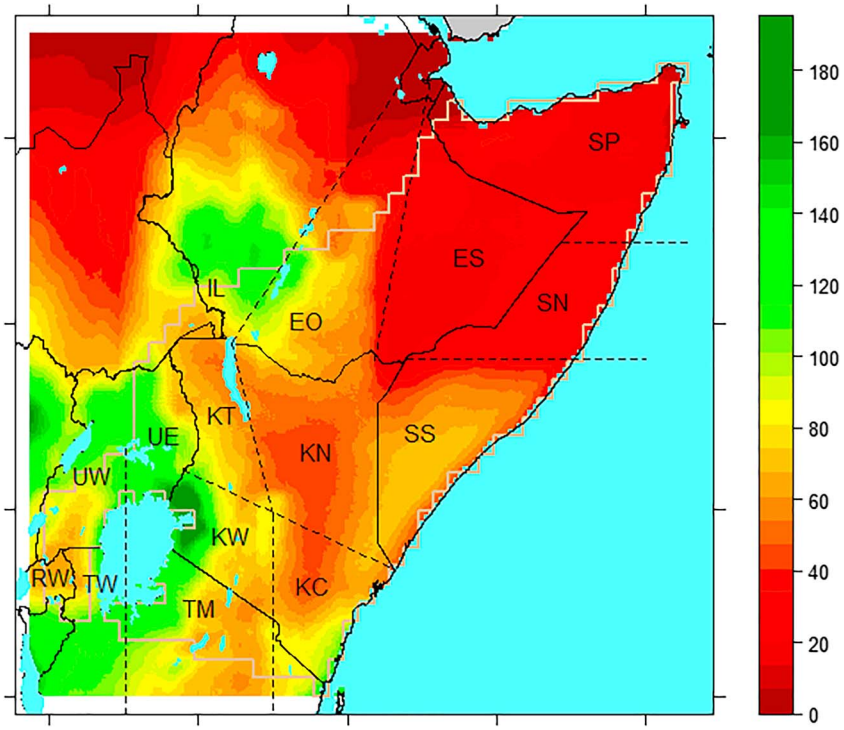

Figure 2. Observed precipitation rates for the 2014 March–May Long Rains season from TAMSAT (Tarnavsky et al., 2014).

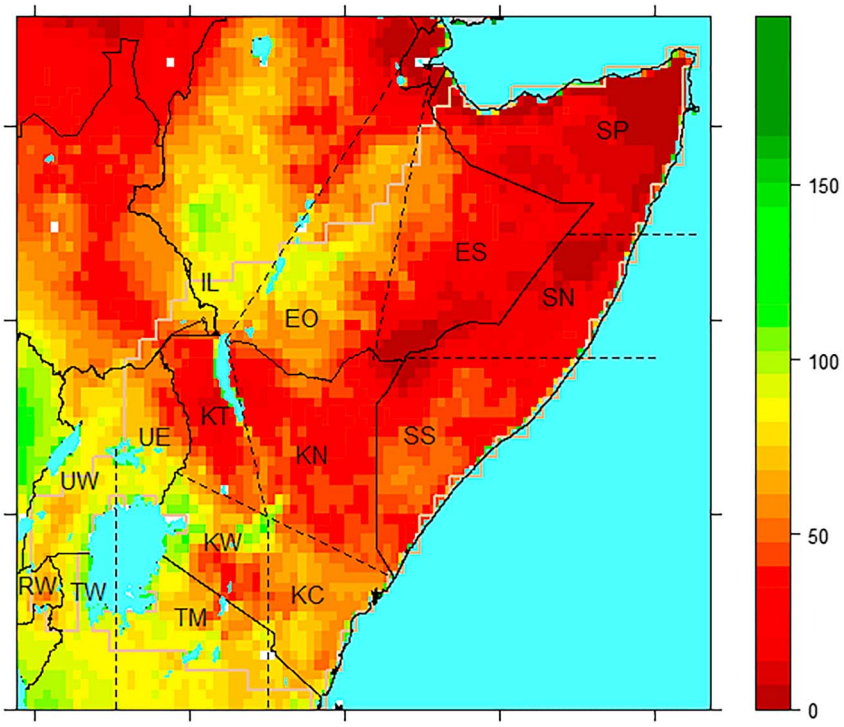

Figure 3. Observed total evapotranspiration rates for the 2014 March–May Long Rains season from GLEAMv3.2a based on reanalysis net radiation and air temperature (ERA-Interim) and MSWEP precipitation, a combination of gauge-based reanalysis, satellite-based precipitation, and satellite-based vegetation optical depth (Martens et al., 2017).

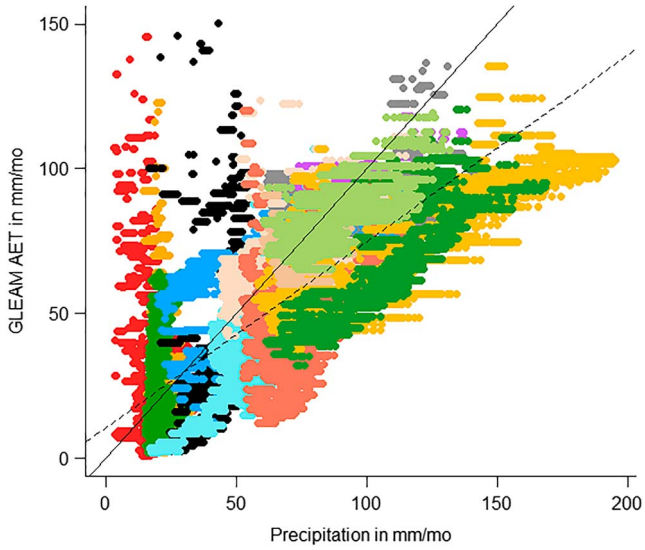

Figure 4. Regression of actual evapotranspiration AET from GLEAM (Figure 3) against precipitation from TAMSAT (Figure 2). Points are from the Greater Horn of Africa bimodal seasonality area only, not the whole Greater Horn of Africa, with points shaded by region (Figure 1). For reference, a 1–1 line is shown (solid) and a linear regression line (broken). Regression equation is (GLEAM AET in mm/mo) = 0.642*(Precipitation in mm/mo) + 10.643 (fit is significant at the 5% level: F test, $F = 187094.6$ on degrees of freedom 1 and 114168).

are the best tool we have to extract information on which factors are related to recent human activities, however such studies remain rare for Africa, partly because of short instrumental records that limit our ability to assign causation with certainty (Stott et al., 2014; Tierney et al., 2013).

Climate event attribution studies investigate the links between climate changes or events and their natural or anthropogenic drivers within the climate system (Hulme, 2014; IPCC, 2014; Marthews et al., 2015; Pall et al., 2011; Trenberth, 2012). The attribution issue gains added urgency because extreme weather events such as heatwaves, floods, and droughts can be associated with high levels of loss and damage to human society (James et al., 2014; Stott et al., 2014; Trenberth et al., 2015).

Although attribution techniques have been applied successfully to climate variables in many studies (Marthews et al., 2015; Pall et al., 2011), very few studies have applied event attribution techniques to land surface components of the energy balance and water balance (Philip et al., 2018; Sippel et al., 2017) and no studies we are aware of have used land surface variables directly calculated from a fully developed and independent land surface model, accessing the much greater reliability of values calculated from a full simulation of the land surface environment rather than estimated from simple energy- or water-balance equations (Long et al., 2014). This is partly because of the technical challenges involved in attributing causes of changes in land surface variables, which involves use of both a climate model and an independent land surface model together across a statistically significant ensemble of driving data. In an African context, these challenges are compounded with relatively low data availability, especially in remote areas such as much of the GHA.

1.2. Land Surface Simulation

The Joint UK Land Environment Simulator (JULES, http://jules.jchmr.org) is a state-of-the-art land surface model that directly calculates energy balance and water balance at each point of the surface every time step (Best et al., 2011; Clark et al., 2011). JULES provides a comprehensive description of the land surface evaporative regime, allowing better simulation of land surface processes and quantification of impacts. JULES has been selected for use in this study because it has been validated comprehensively for global environment simulation, including in tropical environments such as those of the GHA (Marthews et al., 2012).

1.3. Land-Atmosphere Coupling Strength

Land-atmosphere coupling metrics are ways of quantifying how connected land surface dynamics are to the dynamics of the lowest atmospheric layers and thereby effectively summarizing the energy and water balance dynamics of particular locations (Bierkens, 2015; Vidale et al., 2009; Zscheischler & Seneviratne, 2017). The Vegetation-Atmosphere Coupling (VAC) index was introduced by Zscheischler et al. (2015) in order to identify regions and times of concurrent strong anomalies in temperature and photosynthetic activity and to serve as a "conceptual depiction" of the land surface evaporative regime (Figure 5).

In general, regions with strong coupling should respond strongly to meteorological forcings (e.g., precipitation deficit very quickly leads to drought conditions on the surface in terms of decreased evaporation and/or lower soil moisture availability). However, during some seasons and times regional land surfaces may only be weakly coupled to the lower atmosphere (e.g., if wind speeds are high and/or the magnitude of surface water fluxes very low) and in some areas weak coupling may be independent of meteorological conditions (e.g., on particular soil types, Vidale et al., 2009). In "decoupled" regions we would expect to see drought conditions on the surface diverge from collocated areas of precipitation deficit.

The VAC was proposed as a tool to detect when a region tips into a period of water-stress and to quantify stress intensity (Zscheischler et al., 2015), that is, it is suggested as a predictive tool for drought occurrence and impact. It is not suggested that it would have better predictive power than full land surface simulation approaches where these factors are simulated directly, but in a relatively dry climate area such as the GHA it

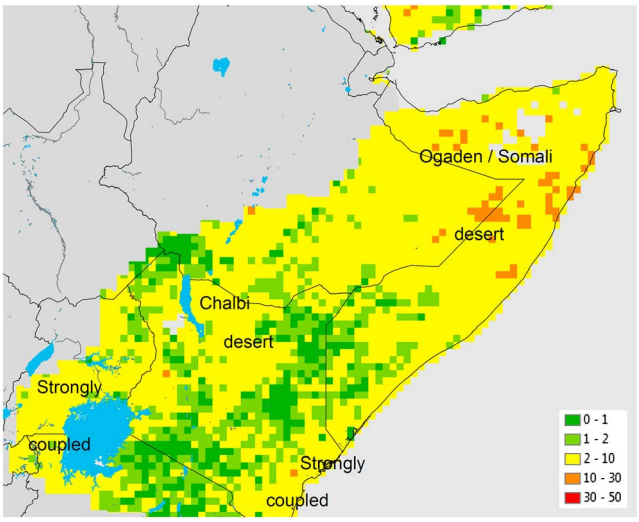

Figure 5. Vegetation-Atmosphere Coupling (VAC) index values from Zscheischler et al. (2015), calculated as the averaged probability of strong coupling over 1982–2011 (from assigning the "strong atmospheric coupling" index values VAC_a and VAC_b a value 100 at each time point during March–May and averaging). This is an index scaled so that higher values mean a higher occurrence of "energy-limited conditions," when atmospheric dynamics dominantly control land surface dynamics (Zscheischler et al., 2015). Note that strong coupling broadly appears to be a feature of desert regions (esp. in the absence of groundwater) and the most humid regions (marked "strongly coupled"), but not intermediate regions (green). For region names see Figure 1.

is possible that the VAC encodes enough predictive information to make time-consuming land surface model simulations less necessary, and we therefore also consider and test this possibility.

In this study we take the year 2014 as our focus. The year 2014 saw depressed rains throughout Kenya and a widespread increase in food insecurity across the region (ECHO, 2014). Across the GHA as a whole precipitation deficit was not extreme, but conditions were extreme for the central part of the GHA (Marthews et al., 2015) and 2014 marked the start of a serious deterioration to drought conditions in Kenya in particular that remains ongoing (2018). Therefore, data from 2014 are anticipated to have high diagnostic value as the year of initiation of deteriorating conditions in the GHA. We ask the following questions:

1. Were the 2014 Long Rains in the GHA significantly different in terms of frequency or coverage, compared to the situation without human-induced climate change?
2. Did the 2014 drought response correlate with areas of high and low VAC index?
3. What are the uncertainties in our current modeling system for predicting drought responses from precipitation changes?

2. Data and Methods

We used Probabilistic Event Attribution techniques (Marthews et al., 2015; Otto et al., 2015; Stott et al., 2014), which involve an ensemble approach to estimating the human contribution to observed changes in the climate system (Massey et al., 2014). Two sets of ensemble simulations were generated for the period December 2013 to December 2014: one *factual* using climate models with present-day greenhouse gases and observed SSTs from the period studied and one *counterfactual* based on the "world that might have been" without higher greenhouse gas emissions (Otto et al., 2015). These counterfactual simulations are generated using the same climate models but with preindustrial greenhouse gases and SSTs (Otto et al., 2015). Comparisons between these two ensembles allow us to quantify the fraction of extreme event probability that is attributable to anthropogenic as opposed to natural drivers (*fraction of attributable risk*, Pall et al., 2011).

Large ensembles of model simulations are necessary for Probabilistic Event Attribution in order to sample the range of extreme climate events that may occur and also diagnose the range of possible event impacts. Our ensembles were derived from repeated runs of the Met Office Hadley Centre Regional Climate Model HadRM3P (developed for the PRECIS modeling system Providing REgional Climates for Impacts Studies, Jones et al., 2004) with boundary conditions provided by the global version of this model HadAM3P (Massey et al., 2014). Observed SSTs were derived from the Operational Sea surface Temperature and sea Ice Analysis (OSTIA) and perturbed initial conditions were drawn from a set of possible perturbations of GCM starting conditions following the method described in Massey et al. (2014). These simulations were then run on volunteer computers through the climate*prediction*.net *weather@home* project (Allen, 1999; Massey et al., 2014).

2.1. Climate Model Suitability

The HadAM3P global climate model is the most appropriate model to be used in this study because it has benefited from a number of optimizations and improvements, including calculation of layered cloud cover, calculation of the radiative effects of convection (slightly reducing the brightness of convective clouds), and modified soil heat conduction under vegetated surfaces. These improvements are fully discussed at a global scale in Massey et al. (2014). Notably for this study, Massey et al. (2014) reported a general improvement in the representation of temperature extrema in HadAM3P.

At regional scale, the HadRM3P model was used over a smaller domain. Following Marthews et al. (2015), we used a 0.44° resolution simulation domain (~50 km at the Equator) covering Africa from 14.3°S to 46.0°N

and from 25.0°W to 62.6°E (i.e., the COordinated Regional Climate Downscaling Experiment (CORDEX) Africa domain cropped at Lilongwe in the south): A much greater area than the GHA (Figure 1) that ensured edge effects were negligible during these simulations. Massey et al. (2014) reported that using the HadAM3P model produced comparable distributions of precipitation bias as its regional variant over Europe. In order to ensure the same comparability over the GHA, modeled precipitation totals over the simulation domain were compared to standard observational data from TAMSAT, CRU-TS, TRMM, and MSWEP using existing *weather@home* simulations covering a 24-year time period (1987–2011) and showed very good agreement compared to precipitation data from the Tropical Applications of Meteorology using SATellite data and ground-based observations project TAMSAT (Tarnavsky et al., 2014), the Climate Research Unit CRU-TS (Mitchell & Jones, 2005), the Tropical Rainfall Measuring Mission TRMM (Dinku et al., 2007) and Multi-Source Weighted-Ensemble Precipitation MSWEP (Beck et al., 2017; see supporting information).

For the JULES simulations (see below), we selected 100 factual and 100 counterfactual ensemble members from the December 2013 to December 2014 simulations via stratified sampling: We examined the distribution of simulated average March to May (long rains) precipitation over the GHA and divided this into 20 bins, from each of which five representative members were randomly chosen (20 bins was an optimal number in order to allow adequate sampling of the tail of low-precipitation simulations within an acceptable run time).

2.2. Land Surface Simulation

The JULES v3.4.1 (Best et al., 2011; Clark et al., 2011) was driven using these climate data to simulate land surface processes and quantify impacts, running at the same resolution and on the same simulation domain. JULES is a grid-based simulator that exists in two forms: *Coupled JULES* where it forms the lower boundary of the UK Met Office Unified Model climate and weather simulator (e.g., HadRM3P incorporates a version of this) and *JULES Standalone* where it solves the land surface energy, water, and other balance equations using driving data supplied separately without any calculation of land-atmosphere feedbacks. Although for long simulations, using coupled JULES is usually preferable because it better constrains the values of the lower atmosphere, JULES Standalone incorporates more sophisticated and exact calculations of surface water and energy fluxes (see Best et al., 2011, and release notes on https://jules.jchmr.org/content/code) that are very desirable for short runs, notably evapotranspiration (Long et al., 2014). Therefore, we used JULES Standalone in this study, entailing a secondary step of offline runs for all ensemble members. The vegetation dynamics module of JULES (called TRIFFID) was activated to allow vegetation carbon pools to be updated but not fractional cover (which was kept fixed) and vegetation parameters were held at standard values for tropical vegetation (following Marthews et al., 2012).

Land surface simulations were carried out in three stages: First, a long spin-up for 100 model years (repeating 2013 *weather@home* data) was conducted with TRIFFID activated to allow soil carbon pools to be equilibrated (Exbrayat et al., 2014). Second, a short spin-up for 30 model years with TRIFFID deactivated and with leaf area index and canopy height prescribed was run in order to equilibrate the soil moisture and temperature stores. Finally, the factual and counterfactual simulations were initiated with no further spin-up (in order to retain transient effects from 2013 conditions) and run for the period December 2013 to December 2014 (leaf area index and canopy height were still prescribed to avoid divergence between ensemble members in these variables). Atmospheric CO_2 concentration was held constant across all simulations.

Drought is routinely measured using a variety of indices (Mishra & Singh, 2010; Vicente-Serrano et al., 2012; Wanders et al., 2010). From these we selected two: First, we followed Seneviratne et al. (2010) and Teuling et al. (2013) in focusing on *ET* as the most critical measure of drought on the land surface. Second, the most standard index of climatological drought, the Standardized Precipitation Index (SPI_{MAM}, Svoboda & Fuchs, 2016), is used as a measure of precipitation deficit (taking 1983–2012 as baseline conditions; n.b. only long rains precipitation March–May is included in the calculation, not annual totals, hence the subscript). All statistical analyses were carried out using R v.3.5.1 (R Development Core Team, 2018).

3. Results

3.1. Validation of Simulated Evapotranspiration

The lack of reliable local measurements from the region mean that only a limited validation of the JULES output evapotranspiration results is possible, based on the global GLEAM data set (Martens et al., 2017).

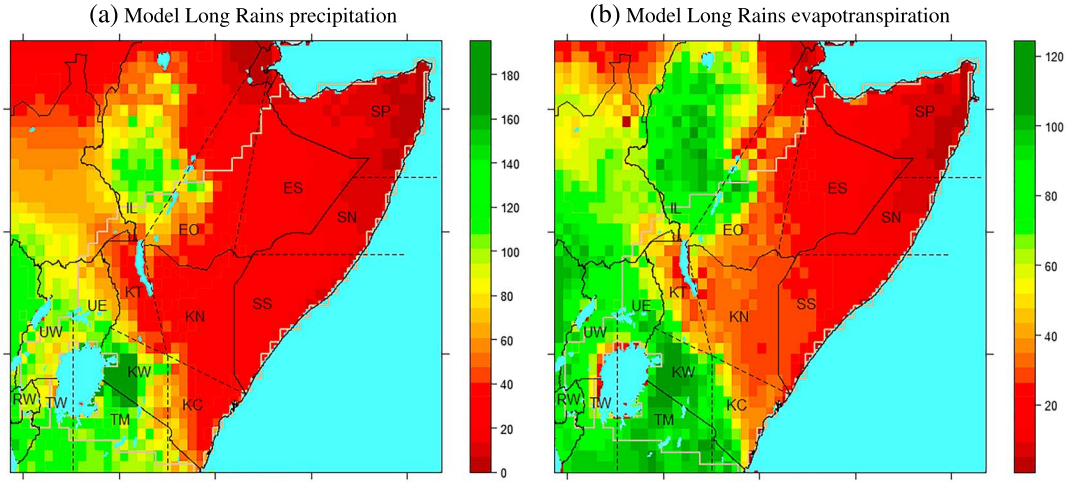

Figure 6. Factual ensemble mean precipitation (a) and evapotranspiration (b) rates for the 2014 March–May Long Rains season. (a) produced by HadRM3P (cf. Figure 2); (b) produced by the Joint UK Land Environment Simulator model (cf. Figure 3).

Simple regression statistics show that in the GHA evapotranspiration from JULES (ensemble mean, Figure 6b) presented a similar relationship with precipitation during the 2014 Long Rains as was presented by GLEAM evapotranspiration (Figure 7, and cf. Figure 4; regression fit F test was highly significant, $F = 193435.7$ on degrees of freedom 1 and 114168). This gives initial support to our results, but evapotranspiration is a particularly problematic variable that is not directly detectable by satellites (Martens et al., 2017), so some understanding of the uncertainties in both the JULES and GLEAM data is necessary to show that these results are indeed robust enough to reflect real patterns on the ground in the GHA.

Even though GLEAM is based more closely on observational data, it would be incorrect simply to favor GLEAM (Figure 3) over the JULES predictions (Figure 6b) in an uncertainty analysis. First, GLEAM has inherent uncertainties that must be taken into account including (1) a known lack of validation sites from very wet and very dry environments (75% of GLEAM validation stations are located in the Continental United States, so areas of consistently high cloud coverage (as is the case in the GHA during the Long Rains because of the dynamics of the tropical rain belt) and semiarid/arid areas (e.g., the Ogaden/Somali and Chalbi deserts) were not sampled extensively; Martens et al., 2017) and (2) the use of the Priestley-Taylor equation for evapotranspiration which becomes very approximate when convective processes are significant (see Lhomme, 1997; the JULES model uses the more precise Penman-Monteith formulation). Second, although JULES predictions of evaporative flux are not without uncertainties (Best et al., 2011), because they have come from simulations highly constrained against climate model data, are expected to have more consistency with other water cycle quantities (in coupled climate/land surface simulations both land surface and atmospheric variables are constrained by mass balances, but even in standalone simulations water balance is still applied at the land surface) and less uncertainty than remote sensing products in water balance closure terms (Long et al., 2014).

Despite the known issues with GLEAM, however, this data set provides the most reliable existing comparison data at the global scale, so some convergence with GLEAM values is desirable in order to build confidence in our results. Because our JULES evapotranspiration results come from an ensemble, we could calculate an envelope of ensemble uncertainty for each gridcell and define an index *scdiv* to measure the scaled divergence between JULES and GLEAM at each point in the BSA of the GHA:

$$scdiv = (\text{(Ensemble mean of JULES AET values)} - \text{(GLEAM AET)}) / \text{(Ensemble SD of JULES AET values)}.$$

By this measure, in most regions the JULES AET values were within 3.0 standard deviations of the collocated GLEAM estimate (Table 1), which we take as a robust platform on which to base further conclusions. The three most divergent regions were all bordering Lake Nalubaale (Lake Victoria), which may indicate a local anomaly resulting from lake-related dynamics.

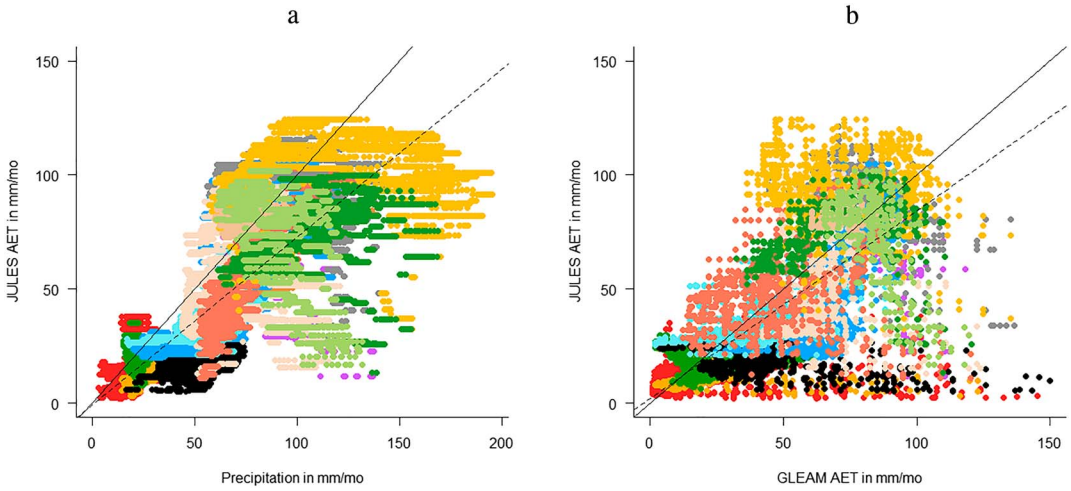

Figure 7. Regressions of actual evapotranspiration AET from JULES (Figure 6b) against precipitation from TAMSAT (Figure 2), and also JULES AET against GLEAM AET (Figure 3). Points are from the Greater Horn of Africa bimodal seasonality area only, not the whole Greater Horn of Africa, with points shaded by region (Figure 1). For reference, 1–1 lines are shown on both plots (solid) and linear regression lines (broken). Regression equations are (a) (JULES AET in mm/mo) = 0.736*(Precipitation in mm/mo) − 0.859 (fit is significant at the 5% level: *F* test, $F = 193435.7$ on degrees of freedom 1 and 114168) and (b) (JULES AET in mm/mo) = 0.825*(GLEAM AET in mm/mo) + 1.760 (fit is significant at the 5% level: *F* test, $F = 125957.4$ on degrees of freedom 1 and 114168). JULES = Joint UK Land Environment Simulator.

3.2. Climate Change in the GHA

There is no doubt that the climate became drier and hotter across the BSA of the GHA in 2014 (Figures 8 and 10) and this is in line with the long-term decline in the long rains across the GHA (Funk et al., 2015; Marthews et al., 2015; Yang et al., 2015). However, our results also point toward subtler shifts in the water and energy balances of particular regions in the GHA that are not explainable as wholly climate-driven responses.

Table 1
Spatial Means (Across the Gridcells Within Each Region) of Evapotranspiration Values From GLEAM and JULES and the Scaled Divergence Between JULES and GLEAM (scdiv)

Region	Spatial mean of GLEAM AET values	Ensemble mean of the spatial mean of JULES AET values (factual ensemble)	Ensemble mean of the spatial mean of JULES AET values (counterfactual ensemble)	Ensemble mean of the spatial mean of *scdiv* (factual ensemble)
RW	71.746	79.888	84.137	2.006 ***
UW	83.492	73.615	74.494	−2.642 ***
TW	88.908	65.238	67.366	−9.573
TM	79.646	93.089	93.896	4.987
UE	71.387	74.058	73.871	0.530 ***
KT	47.222	47.352	47.833	0.016 ***
KW	71.754	96.584	96.309	7.967
IL	82.153	77.013	73.865	−1.173 ***
KN	39.006	32.207	31.478	−0.703 ***
EO	64.049	45.478	44.634	−2.766 ***
KC	64.295	53.769	53.142	−0.954 ***
SS	40.703	21.675	18.972	−2.466 ***
ES	28.178	18.772	17.505	−1.553 ***
SN	18.091	11.979	11.313	−1.298 ***
SP	18.306	9.264	8.460	−2.688 ***

Note. Scaled divergences <3.0 in absolute value are marked "***" to indicate that in these regions the JULES and GLEAM estimates coincide relatively closely. Note that the values for JULES AET correspond to the vertical coordinates of the arrow start- and end-points in Figure 8. For region names, see Figure 1. JULES = Joint UK Land Environment Simulator.

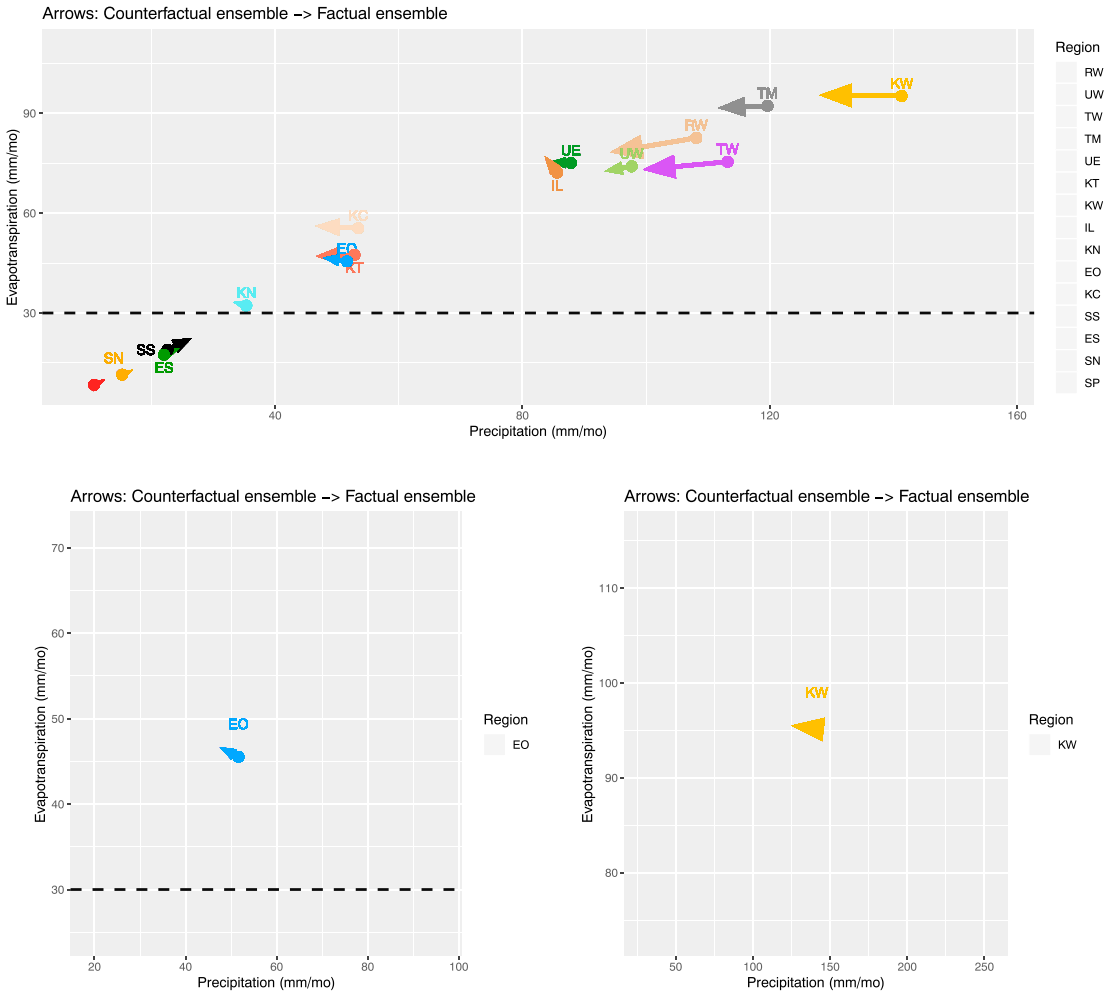

Figure 8. Human-induced climate change is causing wetter sites to become drier and drier sites to become wetter in this part of Africa. Arid and semiarid areas (defined as precipitation<30 mm/mo and/or ET < 30 mm/mo) are remaining stable or becoming slightly wetter, while all other regions are becoming drier. Arrows run from counterfactual to factual ensemble means (after spatial averages over all grid cells within each region have been taken for each ensemble member). Note that the vertical coordinates of arrow start- and end-points correspond to the values for Joint UK Land Environment Simulator AET in Table 1. For region names, see Figure 1. (insets) Regions EO and KW have been expanded to show ensemble spread more clearly: Each arrow displayed connects the ensemble counterfactual mean to the ensemble factual mean, calculated as the centroids of the start- and end-points of the ensemble members. Ensemble spread is displayed by shading (light shading for the spread of 50% of start points and darker shading for the spread of 50% of end points). For the two insets, each ensemble member is additionally shown as a smaller arrow.

Human-induced climate change in the GHA is causing wetter sites to become drier and drier sites to become wetter whether measured in terms of precipitation (Figure 8), evapotranspiration (Figure 8), or Standardized Precipitation Index (Figure 10). This trend is the opposite of the wet-get-wetter, dry-get-drier paradigm for global and regional climate changes of Chou et al. (2013), which would have modified our Figure 8 into a divergent plot, for example, but we note that our regions are smaller than those of that study and therefore more susceptible to local effects (e.g., small scale shifts in the tropical rain belt), and also that Chou et al. (2013)'s predictions for the Horn of Africa in particular did not meet their own criteria for significance (95% statistical confidence level), so we do not pursue further comparison with this paradigm.

Human-induced climate change is causing all sites to become warmer (Figure 10) with a general decrease in soil storage of water (Figure 11). Regarding drought occurrence within these biomes, regions shaded brown on Figure 9 have decreased return times in the factual ensemble (Table 2; i.e., drought occurs more often; the brown line is leftmost on the equivalent return time plot, e.g., KT on Figure S2) and regions shaded mostly blue have increased return times in the factual ensemble (i.e., drought occurs less often; the brown line is

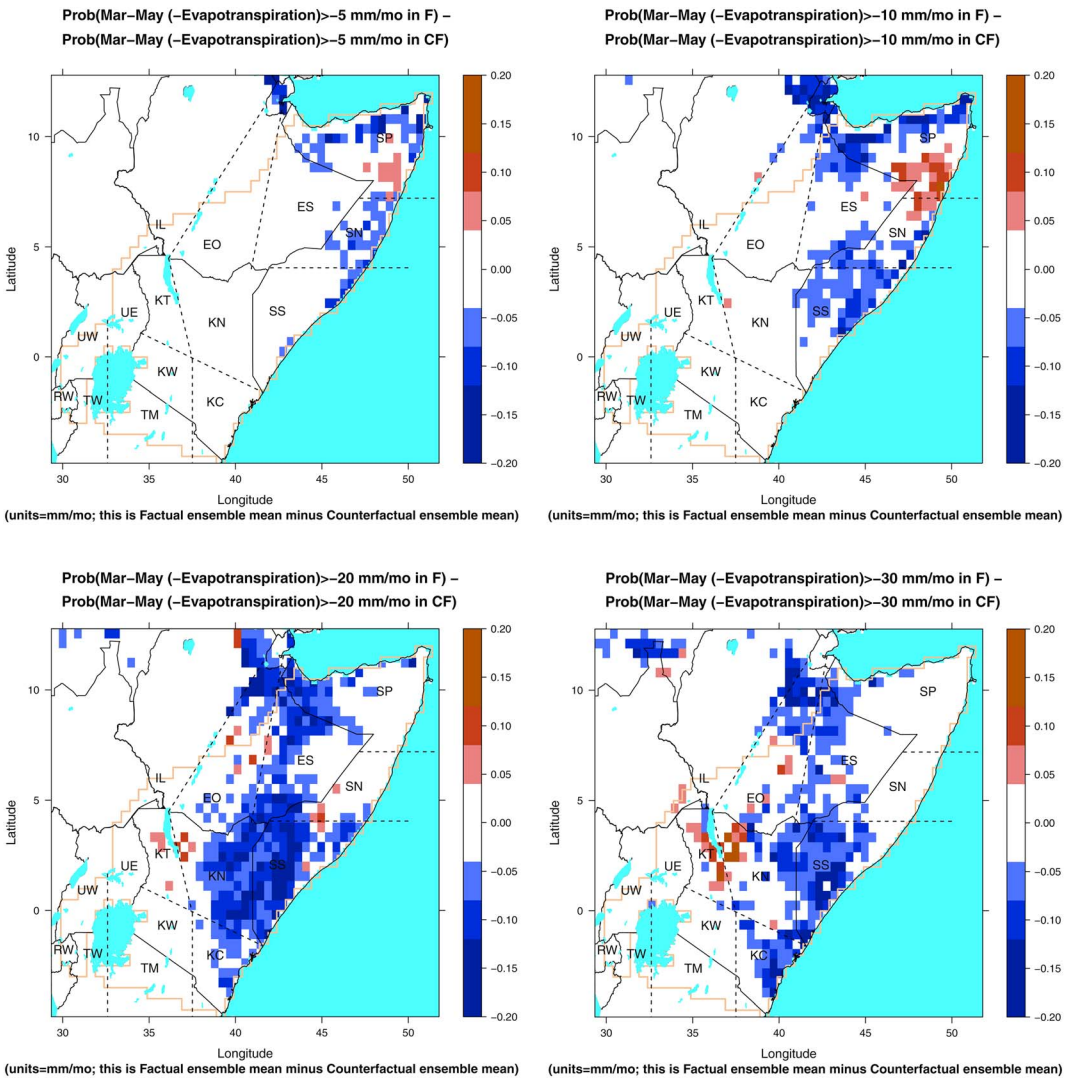

Figure 9. Plot shows factual ensemble mean *P* minus counterfactual ensemble mean *P*, where *P* is the long rains average probability of evapotranspiration rate (*ET*) dropping below four different thresholds ranging from dry (<30 mm/mo) to very dry (<5 mm/mo) conditions. In 2014, areas shaded brown showed an increase in the occurrence of low *ET* that is attributable to human-induced climate change, whereas areas shaded blue showed a decreasing occurrence of low *ET* (and remaining areas showed no change, either because *ET* is always lower or always above the threshold). For region names, see Figure 1.

rightmost on the equivalent return time plot, e.g., SS on Figure S2). Therefore, we identify the area around Lake Turkana, Kenya, as a hot spot for increasing drought occurrence defined as AET < 30 mm/mo during the Long Rains, and also the eastern Ogaden/Somali desert, Somalia-Puntland as a hot spot for increasing drought occurrence defined as AET < 10 mm/mo (severe drought) during the Long Rains (Figure 9).

3.3. Shifts in Drought-Affected Areas in the GHA Resulting From Anthropogenic Climate Change

Marthews et al. (2015) drew attention to possible anthropogenic influence in the development of drought conditions during the East African long rains in 2014. In our analysis we reinforce this conclusion, but additionally find sharp regional differences in the magnitude of the simulated anthropogenic influence on drought. The results show regional variation in the influence on precipitation and evapotranspiration, with changes over coherent subregions moving in different directions (Figure 8). In particular, these results suggest the influence of human-induced climate change in this season was to move regions from Lake Nalubaale (Lake Victoria) to Northern Kenya toward a regime of less precipitation but unchanged evaporation, while moving Eastern Ethiopia, Southern Somalia, and coastal Kenya toward less dry conditions (though with little influence on the most arid parts of the Ogaden/Somali desert). This suggests a fragmentation into two

Table 2
Drought Return Times, Defined as Evapotranspiration Rate Dropping Below the Given Threshold Values, Across the Horn of Africa

	Return times (years) for conditions drier than four threshold Long Rains evapotranspiration rates			
Region	5 mm/mo	10 mm/mo	20 mm/mo	30 mm/mo
RW	-	-	-	-
UW	-	-	-	21.0 → 20.8
TW	-	-	-	-
TM	22.5 → 22.5	22.5 → 22.5	22.5 → 22.5	22.5 → 22.5
UE	-	-	-	36.8 → 36.5
KT	19.0 → 19.0	18.5 → 18.5	14.1 → 13.5	7.8 → 7.1
KW	38.0 → 38.0	38.0 → 38.0	38.0 → 38.0	38.0 → 38.
IL	-	-	-	9.6 → 11.0
KN	67.9 → 56.4	30.9 → 48.1	17.8 → 23.6	11.1 → 10.8
EO	-	20.6 → 59.3	16.3 → 15.0	7.9 → 8.7
KC	-	27.8 → 25.6	18.1 → 15.8	11.2 → 10.8
SS	27.9 → 30.4	14.0 → 19.3	3.0 → 4.3	1.3 → 1.7
ES	40.9 → 34.5	22.8 → 20.2	2.7 → 2.8	1.1 → 1.3
SN	35.6 → 37.3	12.0 → 12.8	1.2 → 1.3	1.0 → 1.0
SP	4.9 → 5.4	2.0 → 2.0	1.1 → 1.1	1.0 → 1.0

Note. Times for four threshold rates are shown (see Figure 9 for maps of these thresholds and Figure S2 for curves of all possible threshold rates), with the time calculated from the counterfactual ensemble (before the "→") and the factual ensemble ("-" means this level of dryness does not occur in our ensembles). For example, taking dry conditions in Ethiopia/Oromia (EO) as (mean March–May evapotranspiration) < 10 mm/mo, there has been a shift in occurrence of dry conditions from once every 20.6 years (counterfactual mean) to once every 59.3 years (factual for 2014), which is a decrease in drought occurrence attributable to human-induced climate change. For region names, see Figure 1.

distinct subzones of influence: One where human climate change induces drying trends and one where it induces wetter average conditions, at least in Long Rains seasons with similar characteristics to that of 2014.

The fragmentation of the BSA is shown most clearly by considering probability of occurrence of low evaporative flux (Figure 9). Human-induced climate change is having an attributable effect in the brown- and blue-colored areas across Ethiopia, Kenya, and Somalia in Figure 9: (1) In the brown areas, simulated drought occurrence (as defined by low evapotranspiration during the long rains) in 2014 was increased in comparison to conditions without climate change; (2) in the blue areas, drought occurrence in 2014 was reduced; (3) the regions around Lake Nalubaale (Lake Victoria) where evapotranspiration is usually high (see Figure 8) showed no change in drought occurrence (evaporation rates remained high enough that drought occurrence was still negligible); and (4) the desert regions of Eastern Ethiopia and Northern Somalia where evapotranspiration is usually very low (Figure 8) also showed no change in drought occurrence (effectively, these regions are always in drought irrespective of the effects of human-induced climate change).

Combining our results from average values (Figure 8) and average occurrences (Figure 9), we can identify two distinct "drought trajectories" in the Horn of Africa BSA in our attribution experiments:

1. Trajectory A: A worsening of drought risk as a result of human-induced climate change for the western part of the zone (Rwanda to Kenya North). Within this area, the simulations suggest drought conditions in this season were made more likely in a band from Ethiopia/Oromia south to the northern half of Kenya.
2. Trajectory B: A small reduction in drought risk for the eastern regions of the zone as a result of human-induced climate change. Within this area the simulations suggest drought conditions in this season were made less likely in a band from Ethiopia/Somali to South Somalia to the Kenya coast.

4. Discussion

Drought is not always initiated by a precipitation deficit: Other changes such as an increase in net radiation or temperature can lead initially to increased evaporative demand (Dai, 2013) but then decreased levels of evapotranspiration in the medium-term as soil moisture stores are depleted (i.e., evaporation over land, hereafter *ET*) and also reduced groundwater and stream flow (Gregory et al., 1997; Teuling et al., 2009; Teuling et al.,

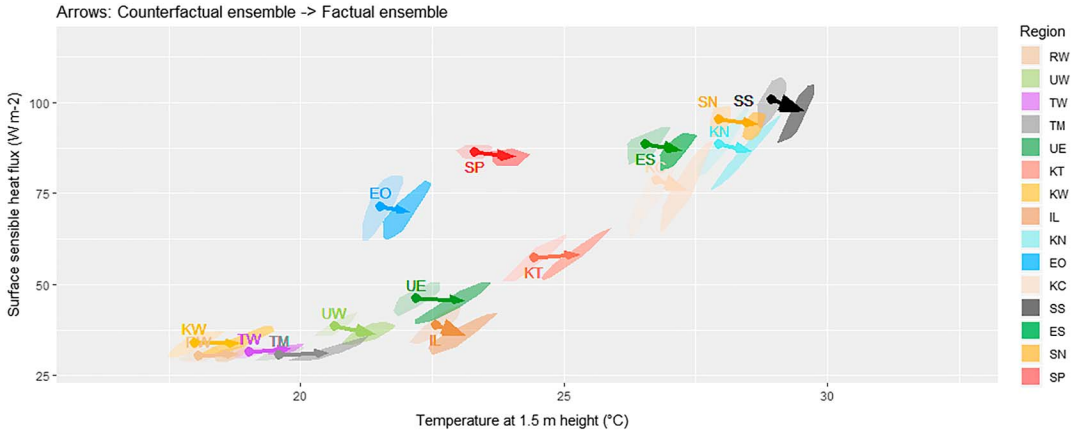

Figure 10. Sensible heat flux and temperatures for the regions of the bimodal seasonality area. Each arrow displayed connects the ensemble counterfactual mean to the ensemble factual mean, calculated as the centroids of the start- and end-points of the ensemble members. Ensemble spread is displayed by shading (light shading for the spread of 50% of start points and darker shading for the spread of 50% of end points). For region names, see Figure 1.

2013). The dominant type of evaporation regime occurring at a particular location, the land surface energy and water balance, and how drought impacts are mediated through the landscape are all crucial for understanding the dynamics of drylands and other ecosystems (Dai, 2013; Seneviratne et al., 2010).

4.1. Attribution of the 2014 Long Rains in the GHA

Anthropogenic climate change has resulted in a complex pattern of change in precipitation and drought risk across the GHA (Figure 1) during the Long Rains season of 2014. Two distinct drought trajectories are apparent within the BSA in the GHA that are attributable to human-induced climate change: a worsening of drought in the west (Trajectory A) and a small reduction in drought risk in the northeast (Trajectory B). These trajectories had the effect of slightly fragmenting the BSA during 2014 and suggest that the response to external climate anomalies is becoming less uniform across the subcontinental region.

What are the driving anthropogenic mechanisms behind these regional wetting and drying patterns? The most universal signal we see for the region in 2014 is that all regions were getting warmer (Figure 10). We suggest that this warming was enough to counteract the negative IOD phase that occurred in 2014 (which brought cooler SSTs; q.v. ss.4.4). The tropical rain belt (Nicholson, 2017, 2018), which controls the annual bimodal rainfall regime in the GHA (Bierkens, 2015; Funk et al., 2014; Lyon & DeWitt, 2012; Yang et al., 2014), appears to have shifted toward the coast of the GHA. In this study we used modeled evapotranspiration derived from simulations with fixed vegetation cover, so we note that biome transitions and vegetational shifts might have acted to exacerbate these trends, and that our estimates of drought occurrence in 2014 (Figure 9) should be taken as parsimonious in this sense.

4.2. Land-Atmosphere Coupling Strength in the GHA

Teuling et al. (2009) and Teuling et al. (2013) found that increased radiation and reduced cloud cover during summer droughts in Europe led to increased, rather than decreased, *ET* rates because soil moisture was not limiting. They suggested that in many regions radiation might control changes in evaporation rates rather than precipitation, and this concept has been developed through the VAC index of Zscheischler et al. (2015) which attempts to identify global areas that are “energy-limited” in this way rather than “soil moisture-limited” (Figure 5).

In our study area of the GHA, however, we found that the VAC index only correlated with some drought-affected areas in 2014 (Figures 5 and 9). Consideration of the theoretical basis of the VAC does make it clear why this should be so in an area with a wide occurrence of hyperarid and desert (xeric) conditions: Moving from high-precipitation (hydric) to medium-precipitation (mesic) regions, there is usually a shift from energy-limitation to soil moisture-limitation in the photosynthetic response of plants (on which the VAC is based, Zscheischler et al., 2015), with mesic environments responding predominantly to precipitation changes and hydric environments responding predominantly to changes in radiation input.

However, in tropical environments there are usually three regimes at play rather than just two, because in moving from mesic to xeric regions there is another shift: In this case to a regime where soil moisture levels are no longer dominated by precipitation inputs because precipitation is effectively absent, and in these environments evaporation rates become again dominated by the radiation environment. As is well known, evapotranspiration rates always have a component of radiation-dependence in any environment (guaranteed by the Penman-Monteith equation, Monteith & Unsworth, 1990). In mesic environments this is masked by an overriding signal from daily and seasonal variation in precipitation, but in both hydric environments (where precipitation is high enough that photosynthesis is effectively always at its maximum rate) and xeric environments (where precipitation is low enough to be negligible) the basic vegetational response to radiation becomes dominant. Therefore, mesic environments map to Zscheischler et al. (2015)'s soil moisture-limited state and both hydric and xeric environments map to their energy-limited state. Zscheischler et al. (2015) were aware of this because they masked out several deserts from their published product (e.g., the Sahara), but the xeric environments of the GHA were not considered dry enough to be masked out in this way.

Therefore, VAC values in the GHA are of use in delineating the mesic environments (approximately the eastern shore of Lake Nalubaale (Lake Victoria) to the Ogaden/Somali desert, Figure 5), that is, environments where precipitation and actual evapotranspiration approximately correlate. However, because xeric environments are not differentiable from hydric environments solely by using the VAC (Figure 5), the utility of this index in tropical drought studies is limited outside mesic areas.

4.3. Uncertainties in Our Modeling System

There has recently been significant progress in understanding climate processes, land surface processes, and their interactions via land-atmosphere feedbacks (Dadson et al., 2013; Guillod et al., 2015; IPCC, 2014; Seneviratne et al., 2010; Zscheischler & Seneviratne, 2017). Simulating the causal chain from climatological drought to land surface impacts involves a challenging integration of theory from climate science with other areas such as hydrology, boundary layer meteorology, and land surface physics (Yang et al., 2014, 2015). Additionally, many land surface processes remain poorly understood at the high resolutions required to address issues of local and regional impact (Dadson et al., 2013; Marthews et al., 2015).

Therefore, in this paper we have taken an approach based on land surface modeling, that is, moving from precipitation deficit to drought impact and evaporation. In our simulations, uncertainties naturally existed at many points of the modeling system. Land surface simulation uncertainty has been much-discussed in the literature, for example, in general; for the JULES model in particular see Marthews et al. (2012) and for evapotranspiration specifically see Robinson et al. (2017). The method used by JULES to deduce evaporative flux at the land surface under input precipitation and temperature is standard and based on a Penman-Monteith approach for potential evapotranspiration (Monteith & Unsworth, 1990) modified with a soil water stress factor based on the soil moisture content derived from a Darcy-Richards equation representation of soil hydraulics (Best et al., 2011; Clark et al., 2011). This approach is used by every globally run land surface model included in the current CMIP6 model intercomparison and performs exceptionally well, with uncertainty in land surface model-derived evapotranspiration values being generally much lower than the uncertainty in comparable remote-sensing and GRACE-inferred evapotranspiration rates (Long et al., 2014).

4.4. Regional Variations in Response to Anthropogenic Forcing and the "East African Discrepancy"

The Long Rains (March–May) in the GHA have been in decline since 1999 (Figure 12), which some observers have linked to an upward trend of SSTs in the central Indian Ocean that has been observed over the past several decades (Funk et al., 2014; Funk et al., 2015; Nicholson, 2017), operating through changes in the annual movement of the tropical rain belt and related areas of deep convection (Nicholson, 2017, 2018). Paleoclimatic data show that "century-scale monsoon weakening events" have occurred in the past in East Africa (Kiage & Liu, 2016) and it is therefore possible that we are witnessing the early signs of such a climatic shift. However, most current model simulations predict the long rains to increase in response to anthropogenic greenhouse gas forcing—leading to the so-called East African discrepancy (e.g., Tierney et al., 2013; Boulter et al., 2013; Rowell et al., 2015; Yang et al., 2015; see discussion in Yang & Huntingford, 2018). Yang et al. (2014) even suggested that the cause of this discrepancy was "systematic

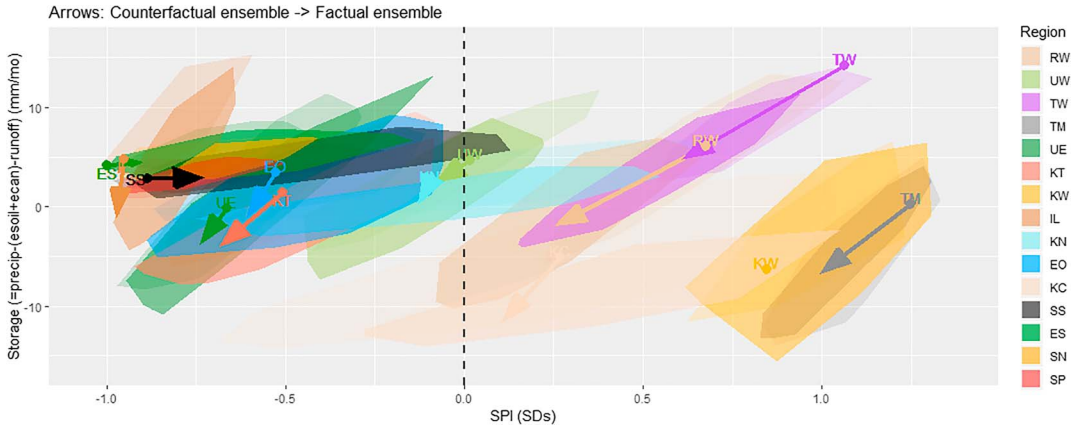

Figure 11. Changes in soil storage of water (=precipitation-ET-runoff) against Standardized Precipitation Index in the March–May season (SPI_{MAM}, WMO & GWP 2016) from the counterfactual ensemble (start of arrow) to the factual ensemble (end of arrow) for the study regions. Each arrow displayed connects the ensemble counterfactual mean to the ensemble factual mean, calculated as the centroids of the start- and end-points of the ensemble members. Ensemble spread is displayed by shading (light shading for the spread of 50% of start points and darker shading for the spread of 50% of end points). For region names, see Figure 1. Note that permanently arid regions (deserts) usually have evapotranspiration (ET) <1 mm/day and in this region of the plot SPI_{MAM} values must be interpreted with caution because mean precipitation values are very low and precipitation events mostly episodic (e.g., an arid location with zero precipitation most years and one precipitation event during the baseline 1983–2012 will post negative SPI_{MAM} values for most years thereafter because mean baseline precipitation will be nonzero). As a result of this, SPI_{MAM} values for SP, SN, and ES are most probably artificially low in this data set.

errors" in fully coupled models trying to simulate the East African precipitation climatology, concluding that "we are distressingly far from an adequate understanding or a usable ability to model climate variability and change in this socially critical region."

Because our results and analysis are restricted to a single year, we can only speculate about long-term trends in the intensity of the long rains, but our results nevertheless can offer some much-needed clarification about the dynamics of precipitation and evaporation in this area and where errors might be arising. First, our finding of two distinct drought trajectories in the Horn of Africa BSA shows that it is insufficient to analyze trends in variables averaged over the whole of this subcontinental area: A finer-scale, more regionalized approach is necessary. Varying definitions of "East Africa" also introduce unnecessary uncertainty: for

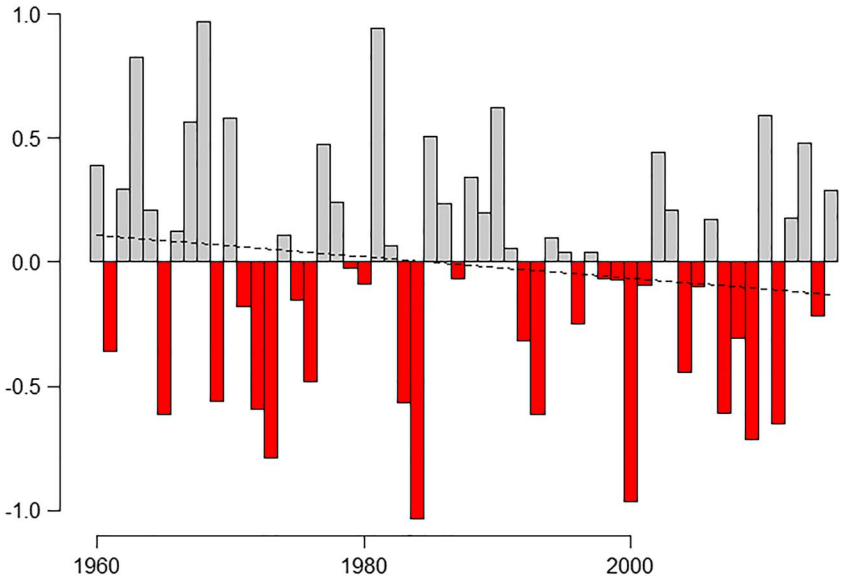

Figure 12. Time series of East African Long Rains (March to May) rainfall for the Greater Horn of Africa bimodal seasonality area. Values represent a regionally averaged standardized departure from the seasonal mean (redrawn from Nicholson, 2017; reproduced with permission from the American Geophysical Union and S. Nicholson).

example, between Lyon and DeWitt (2012), Funk et al. (2014), and Yang et al. (2015), some not only excluded the western half of our BSA, but also included much of the GHA outside the BSA. Although legitimate in individual studies, these geographical choices will greatly affect the robustness of the conclusions drawn about long-term trends.

Second, current global climate models and observational data sets remain limited in the areas of tropical precipitation and convection processes. This is partly because of the greater significance in the tropics of subgrid scale processes (e.g., the seeding of convective storms, Taylor et al., 2012; Trenberth et al., 2015), but also because of observational limitations (e.g., low-level, nonprecipitating cloud occurrence is high in the GHA, Liu et al., 2008, which are not usually detectable by satellites such as *CloudSat*, Liu et al., 2015, and therefore excluded from cloud climatologies used to constrain climate models). There was a negative IOD phase in 2014, meaning cold seas off the shore of East Africa, which usually implies reduced cloud cover inland (acting to decrease both precipitation and evaporation), but our results show that many coastal areas especially in Somalia actually experienced slight increases in both precipitation and evapotranspiration (Figure 8).

Possibly, the reduction in off-shore SST was sufficient to form a "cold tongue complex" pushing the area of atmospheric convergence, and the continental rainband, further inland (similar to what happens at regional scale on the Guinea Coast, West Africa: see Okumura & Xie, 2004). This is supported by the fact that in 2014, despite the reduction in precipitation due to climate change, most inland areas were relatively wet (SPI_{MAM} values, Figure 11). Such a cold tongue effect would leave only low-level, nonprecipitating "warm clouds" at the coast (e.g., see Liu et al., 2015) bringing higher longwave radiation, more warming of the land surface, and higher evaporation rates (see Liu et al., 2008; Luo et al., 2017). This mechanistic chain may also explain why the GHA is thought to only respond weakly to negative IOD events (Williams & Hanan, 2011).

In summary, we suggest a more nuanced conclusion than that of Yang et al. (2014): the above-mentioned limitations on global climate models are well known, but perhaps "adequate understanding" is not as distressingly far away as it appears. The East African discrepancy may eventually simply be solved by ongoing improvements in spatial resolution and observational data sets and more regionally detailed studies of the effects of natural and anthropogenic drivers of climate variability and change Figure 12.

5. Conclusions

Drought is an endemic part of life in the Horn of Africa (ECHO, 2014) and Kenya, Ethiopia and Somalia are all currently drought-affected countries (Kenya continually since 2014, GHACOF, 2018). It is of paramount importance for climate scientists to improve our ability to predict the impacts of climate change in the GHA. In this study we have shown that anthropogenic climate change may have resulted in a complex pattern of change in precipitation and drought risk across the Horn of Africa in the Long Rains season of 2014. Evidence exists for new, distinct responses within the BSA in the GHA. The use of land surface simulations to derive these results is crucial and presents a much clearer assessment of regional responses in these data-poor regions than may be obtained from use of more basic indices that summarize energy and water balance at particular locations, such as the widely used VAC index. We suggest that changes in drought dynamics and related water cycle impacts may only be assessed reliably through attribution studies that include and address changes in land surface variables.

The Horn of Africa is noted for combining complex topography with strong convection effects, resulting in a highly heterogeneous general precipitation climatology (Nicholson, 2017). Together with the challenges of a data-poor part of the world and a high proportion of the population being dependent on rain-fed agriculture (Yang & Huntingford, 2018), the importance of deriving strong and clear conclusions about drought occurrence in the subcontinent is very clear. The paradigm presented here, showing a simple, regional-scale directional pattern that summarizes the changes that we may expect from anthropogenic climate change, should help local populations to become more aware of the importance of future climate trajectories and, therefore, to be more prepared for future drought in this part of Africa. It also suggests that a more detailed regional analysis of precipitation variability and trends and their drivers may help to explain the apparent paradox of a negative trend in East African rainfall over the recent past compared to climate model projections of a wetter future in this region.

Acknowledgments

This research was funded by the Natural Environment Research Council (NERC) NE/K006479/1 to the Attribution of Climate-related Extremes in Africa (ACE-Africa) project, Univ. Oxford. Many thanks to the *weather@home* project, http://www.climateprediction.net/, for providing climate data for the land surface simulations. R. G. J. gratefully acknowledges funding from the Joint Department of Energy and Climate Change (DECC) and Department for Environment Food and Rural Affairs (Defra) Met Office Hadley Centre Climate Programme—DECC/Defra (GA01101). Many thanks to Eleanor Blyth and Chris Taylor for very useful discussions during the development of this paper and also to Jakob Zscheischler for providing Vegetation-Atmosphere Coupling index values. The scripts and associated files used to perform this analysis are uploaded in a Github repository at https://github.com/soi521/JEAfr for unrestricted public download and non-commercial use (please email T. R. M. with any queries).

References

Allen, M. (1999). Do-it-yourself climate prediction. *Nature*, *401*(6754), 642–642. https://doi.org/10.1038/44266

Beck, H. E., van Dijk, A. I. J. M., Levizzani, V., Schellekens, J., Miralles, D. G., Martens, B., & de Roo, A. (2017). MSWEP: 3-hourly 0.25° global gridded precipitation (1979–2015) by merging gauge, satellite, and reanalysis data. *Hydrology and Earth System Sciences*, *21*(1), 589–615. https://doi.org/10.5194/hess-21-589-2017

Best, M. J., Pryor, M., Clark, D. B., Rooney, G. G., Essery, R. . L. H., Ménard, C. B., et al. (2011). The Joint UK Land Environment Simulator (JULES), model description—Part 1: Energy and water fluxes. *Geoscientific Model Development*, *4*(3), 677–699. https://doi.org/10.5194/gmd-4-677-2011

Bierkens, M. F. P. (2015). Global hydrology 2015: State, trends, and directions. *Water Resources Research*, *51*, 4923–4947. https://doi.org/10.1002/2015WR017173

Boulter, S., Palutikof, J., Karoly, D. J., & Guitart, D. (2013). *Natural disasters and adaptation to climate change*. New York: Cambridge University Press.

Chou, C., Chiang, J. C. H., Lan, C., Chung, C., Liao, Y., & Lee, C. (2013). Increase in the range between wet and dry season precipitation. *Nature Geoscience*, *6*, 263–267. https://doi.org/10.1038/NGEO1744

Clark, D. B., Mercado, L. M., Sitch, S., Jones, C. D., Gedney, N., Best, M. J., et al. (2011). The Joint UK Land Environment Simulator (JULES), model description—Part 2: Carbon fluxes and vegetation dynamics. *Geoscientific Model Development*, *4*(3), 701–722. https://doi.org/10.5194/gmd-4-701-2011

Dadson, S., Acreman, M., & Harding, R. (2013). Water security, global change and land-atmosphere feedbacks. *Philosophical Transactions. Series A, Mathematical, Physical, and Engineering Sciences*, *371*(2002), 20120412). https://doi.org/10.1098/rsta.2012.0412

Dai, A. (2013). Increasing drought under global warming in observations and models. *Nature Climate Change*, *3*, 52–58. https://doi.org/10.1038/nclimate1633

Dinku, T., Ceccato, P., Grover-Kopec, E., Lemma, M., Connor, S. J., & Ropelewski, C. F. (2007). Validation of satellite rainfall products over East Africa's complex topography. *International Journal of Remote Sensing*, *28*(7), 1503–1526. https://doi.org/10.1080/01431160600954688

ECHO (2014). Humanitarian implementation plan (HIP) 2015 Horn of Africa*Rep*., European Commission Directorate-General for Humanitarian Aid and Civil Protection (ECHO), Brussels, Belgium.

Exbrayat, J. F., Pitman, A. J., & Abramowitz, G. (2014). Response of microbial decomposition to spin-up explains CMIP5 soil carbon range until 2100. *Geoscientific Model Development*, *7*(6), 2683–2692. https://doi.org/10.5194/gmd-7-2683-2014

Funk, C., Hoell, A., Shukla, S., Bladé, I., Liebmann, B., Roberts, J. B., et al. (2014). Predicting East African spring droughts using Pacific and Indian Ocean sea surface temperature indices. *Hydrology and Earth System Sciences*, *18*(12), 4965–4978. https://doi.org/10.5194/hess-18-4965-2014

Funk, C., Shukla, S., Hoell, A., & Livneh, B. (2015). Assessing the contributions of East African and west Pacific warming to the 2014 boreal spring East African drought. *Bulletin of the American Meteorological Society*, *96*(12), S77–S82. https://doi.org/10.1175/Bams-D-15-00106.1

GHACOF (2018). Mitigation of climate related impacts Rep., Greater Horn of Africa Climate Outlook Forum (GHACOF), Mombasa, Kenya.

Gregory, J. M., Mitchell, J. F. B., & Brady, A. J. (1997). Summer drought in northern midlatitudes in a time-dependent CO2 climate experiment. *Journal of Climate*, *10*(4), 662–686. https://doi.org/10.1175/1520-0442(1997)010<0662:Sdinmi>2.0.Co;2

Guillod, B. P., Orlowsky, B., Miralles, D. G., Teuling, A. J., & Seneviratne, S. I. (2015). Reconciling spatial and temporal soil moisture effects on afternoon rainfall. *Nature Communications*, *6*, Artn 6443. https://doi.org/10.1038/Ncomms7443

Hulme, M. (2014). Attributing weather extremes to 'climate change': A review. *Progress in Physical Geography*, *38*(4), 499–511. https://doi.org/10.1177/0309133314538644

IPCC (2014). Climate change 2014: The physical science basis Rep., Intergovernmental Panel on Climate Change (IPCC), U.K.

James, R., Otto, F., Parker, H., Boyd, E., Cornforth, R., Mitchell, D., & Allen, M. (2014). Characterizing loss and damage from climate change. *Nature Climate Change*, *4*(11), 938–939. https://doi.org/10.1038/nclimate2411

Jones, R. G., Noguer, M., Hassell, D. C., Hudson, D., Wilson, S. S., Jenkins, G. J., & Mitchell, J. F. B. (2004). *Generating high resolution climate change scenarios using PRECIS*. Exeter, U.K: Met. Office Hadley Centre.

Kiage, L. M., & Liu, K.-b. (2016). Late Quaternary paleoenvironmental changes in East Africa: A review of multiproxy evidence from palynology, lake sediments, and associated records. *Progress in Physical Geography*, *30*(5), 633–658. https://doi.org/10.1177/0309133306071146

Lhomme, J.-P. (1997). An examination of the Priestley-Taylor equation using a convective boundary layer model. *Water Resources Research*, *33*(11), 2571–2578. https://doi.org/10.1029/97WR01897

Liu, D., Liu, Q., & Zhou, L. (2015). Underestimation of oceanic warm cloud occurrences by the Cloud Profiling Radar aboard CloudSat. *Journal of Meteorological Research*, *29*(4), 576–593. https://doi.org/10.1007/s13351-015-5027-5

Liu, Q., Fu, Y., Yu, R., Sun, L., & Lu, N. (2008). A new satellite-based census of precipitating and nonprecipitating clouds over the tropics and subtropics. *Geophysical Research Letters*, *35*, L07816. https://doi.org/10.1029/2008GL033208

Long, D., Longuevergne, L., & Scanlon, B. R. (2014). Uncertainty in evapotranspiration from land surface modeling, remote sensing, and GRACE satellites. *Water Resources Research*, *50*, 1131–1151. https://doi.org/10.1002/2013WR014581

Luo, Z. J., Anderson, R. C., Rossow, W. B., & Takahashi, H. (2017). Tropical cloud and precipitation regimes as seen from near-simultaneous TRMM, CloudSat, and CALIPSO observations and comparison with ISCCP. *Journal of Geophysical Research: Atmospheres*, *122*, 5988–6003. https://doi.org/10.1002/2017JD026569

Lyon, B. (2014). Seasonal drought in the Greater Horn of Africa and its recent increase during the March–May long rains. *Journal of Climate*, *27*(21), 7953–7975. https://doi.org/10.1175/jcli-d-13-00459.1

Lyon, B., & DeWitt, D. G. (2012). A recent and abrupt decline in the East African long rains. *Geophysical Research Letters*, *39*, L02702. https://doi.org/10.1029/2011GL050337

Martens, B., Miralles, D. G., Lievens, H., van der Schalie, R., de Jeu, R. A. M., Fernández-Prieto, D., et al. (2017). GLEAM v3: Satellite-based land evaporation and root-zone soil moisture. *Geoscientific Model Development*, *10*(5), 1903–1925. https://doi.org/10.5194/gmd-10-1903-2017

Marthews, T. R., Malhi, Y., Girardin, C. A., Silva Espejo, J. E., Aragão, L. E., Metcalfe, D. B., et al. (2012). Simulating forest productivity along a neotropical elevational transect: Temperature variation and carbon use efficiency. *Global Change Biology*, *18*(9), 2882–2898. https://doi.org/10.1111/j.1365-2486.2012.02728.x

Marthews, T. R., Otto, F. E. L., Mitchell, D., Dadson, S. J., & Jones, R. G. (2015). The 2014 drought in the Horn of Africa: Attribution of meteorological drivers. *Bulletin of the American Meteorological Society*, *96*(12), S83–S88. https://doi.org/10.1175/bams-d-15-00115.1

Masih, I., Maskey, S., Mussá, F. E. F., & Trambauer, P. (2014). A review of droughts on the African continent: A geospatial and long-term perspective. *Hydrology and Earth System Sciences*, *18*(9), 3635–3649. https://doi.org/10.5194/hess-18-3635-2014

Massey, N., Jones, R., Otto, F. E. L., Aina, T., Wilson, S., Murphy, J. M., et al. (2014). weather@home—Development and validation of a very large ensemble modelling system for probabilistic event attribution. *Quarterly Journal of the Royal Meteorological Society*, *141*(690), 1528–1545. https://doi.org/10.1002/qj.2455

Mishra, A. K., & Singh, V. P. (2010). A review of drought concepts. *Journal of Hydrology*, *391*(1–2), 202–216. https://doi.org/10.1016/j.jhydrol.2010.07.012

Mitchell, T. D., & Jones, P. D. (2005). An improved method of constructing a database of monthly climate observations and associated high-resolution grids. *International Journal of Climatology*, *25*(6), 693–712. https://doi.org/10.1002/joc.1181

Monteith, J. L., & Unsworth, M. H. (1990). *Principles of environmental physics*, (2nd ed.). Butterworth, Oxford, U.K: Academic Press.

Nicholson, S. E. (2017). Climate and climatic variability of rainfall over eastern Africa. *Reviews of Geophysics*, *55*, 590–635. https://doi.org/10.1002/2016RG000544

Nicholson, S. E. (2018). The ITCZ and the seasonal cycle over equatorial Africa. *Bulletin of the American Meteorological Society*, *99*(2), 337–348. https://doi.org/10.1175/bams-d-16-0287.1

Okumura, Y., & Xie, S. P. (2004). Interaction of the Atlantic equatorial cold tongue and the African monsoon. *Journal of Climate*, *17*(18), 3589–3602. https://doi.org/10.1175/1520-0442(2004)017<3589:Iotaec>2.0.Co;2

Otto, F. E. L., Boyd, E., Jones, R. G., Cornforth, R. J., James, R., Parker, H. R., & Allen, M. R. (2015). Attribution of extreme weather events in Africa: A preliminary exploration of the science and policy implications. *Climatic Change*, *132*(4), 531–543. https://doi.org/10.1007/s10584-015-1432-0

Pall, P., Aina, T., Stone, D. A., Stott, P. A., Nozawa, T., Hilberts, A. G., et al. (2011). Anthropogenic greenhouse gas contribution to flood risk in England and Wales in autumn 2000. *Nature*, *470*(7334), 382–385. https://doi.org/10.1038/nature09762

Philip, S. Y., Kew, S. F., Hauser, M., Guillod, B. P., Teuling, A. J., Whan, K., et al. (2018). Western US high June 2015 temperatures and their relation to global warming and soil moisture. *Climate Dynamics*, *50*(7–8), 2587–2601. https://doi.org/10.1007/s00382-017-3759-x

R Development Core Team (2018). *R: A language and environment for statistical computing*, (ed.), Vienna, Austria: R Foundation for Statistical Computing.

Robinson, E. L., Blyth, E. M., Clark, D. B., Finch, J., & Rudd, A. C. (2017). Trends in evaporative demand in Great Britain using high-resolution meteorological data. *Hydrology and Earth System Sciences*, *21*, 1189–1224. https://doi.org/10.5194/hess-2015-520

Rowell, D. P., Booth, B. B. B., Nicholson, S. E., & Good, P. (2015). Reconciling past and future rainfall trends over East Africa. *Journal of Climate*, *28*(24), 9768–9788. https://doi.org/10.1175/jcli-d-15-0140.1

Seneviratne, S. I., Corti, T., Davin, E. L., Hirschi, M., Jaeger, E. B., Lehner, I., et al. (2010). Investigating soil moisture–climate interactions in a changing climate: A review. *Earth-Science Reviews*, *99*(3–4), 125–161. https://doi.org/10.1016/j.earscirev.2010.02.004

Sippel, S., Forkel, M., Rammig, A., Thonicke, K., Flach, M., Heimann, M., et al. (2017). Contrasting and interacting changes in simulated spring and summer carbon cycle extremes in European ecosystems. *Environmental Research Letters*, *12*(7), 075006. https://doi.org/10.1088/1748-9326/aa7398

Stott, P. A., Hegerl, G. C., Herring, S. C., Hoerling, M. P., Peterson, T. C., Zhang, X. B., & Zwiers, F. W. (2014). Introduction to explaining extreme events of 2013 from a climate perspective. *Bulletin of the American Meteorological Society*, *95*(9), S1–S96.

Svoboda, M., and B. A. Fuchs (2016). Handbook of drought indicators and indices Rep., World Meteorological Organization (WMO) and Global Water Patnership (GWP).

Tarnavsky, E., Grimes, D., Maidment, R., Black, E., Allan, R. P., Stringer, M., et al. (2014). Extension of the TAMSAT satellite-based rainfall monitoring over Africa and from 1983 to Present. *Journal of Applied Meteorology and Climatology*, *53*(12), 2805–2822. https://doi.org/10.1175/jamc-d-14-0016.1

Taylor, C. M., de Jeu, R. A., Guichard, F., Harris, P. P., & Dorigo, W. A. (2012). Afternoon rain more likely over drier soils. *Nature*, *489*(7416), 423–426. https://doi.org/10.1038/nature11377

Teuling, A. J., Hirschi, M., Ohmura, A., Wild, M., Reichstein, M., Ciais, P., et al. (2009). A regional perspective on trends in continental evaporation. *Geophysical Research Letters*, *36*, L02404. https://doi.org/10.1029/2008GL036584

Teuling, A. J., van Loon, A. F., Seneviratne, S. I., Lehner, I., Aubinet, M., Heinesch, B., et al. (2013). Evapotranspiration amplifies European summer drought. *Geophysical Research Letters*, *40*, 2071–2075. https://doi.org/10.1002/grl.50495

Tierney, J. E., Smerdon, J. E., Anchukaitis, K. J., & Seager, R. (2013). Multidecadal variability in East African hydroclimate controlled by the Indian Ocean. *Nature*, *493*(7432), 389–392. https://doi.org/10.1038/nature11785

Trenberth, K. E. (2012). Framing the way to relate climate extremes to climate change. *Climatic Change*, *115*(2), 283–290. https://doi.org/10.1007/s10584-012-0441-5

Trenberth, K. E., Fasullo, J. T., & Shepherd, T. G. (2015). Attribution of climate extreme events. *Nature Climate Change*, *5*(8), 725–730. https://doi.org/10.1038/nclimate2657

Vicente-Serrano, S. M., Beguería, S., Lorenzo-Lacruz, J., Camarero, J. J., López-Moreno, J. I., Azorin-Molina, C., et al. (2012). Performance of drought indices for ecological, agricultural, and hydrological applications. *Earth Interactions*, *16*(10), 1–27. https://doi.org/10.1175/2012ei000434.1

Vidale, P. L., A. Verhoef, M. E. Demory, and M. Roberts (2009). Land surface–atmosphere coupling strength in the Hadley Centre GCM: The impact of soil physics. In *ECMWF/GLASS Workshop on Land Surface Modelling*, (ed.), Reading, U.K.

von Buttlar, J., Zscheischler, J., Rammig, A., Sippel, S., Reichstein, M., Knohl, A., et al. (2017). Impacts of droughts and extreme-temperature events on gross primary production and ecosystem respiration: A systematic assessment across ecosystems and climate zones. *Biogeosciences*, *15*(5), 1293–1318. https://doi.org/10.5194/bg-15-1293-2018

Wanders, N., H. A. J. van Lanen, and A. F. van Loon (2010). Indicators for drought characterization on a global scale Rep., Water and Global Change (WATCH).

Williams, C. A., & Hanan, N. P. (2011). ENSO and IOD teleconnections for African ecosystems: Evidence of destructive interference between climate oscillations. *Biogeosciences*, *8*(1), 27–40. https://doi.org/10.5194/bg-8-27-2011

Yang, H., & Huntingford, C. (2018). Drought likelihood for East Africa. *Natural Hazards and Earth System Sciences*, *18*(2), 491–497. https://doi.org/10.5194/nhess-18-491-2018

Yang, W., Seager, R., Cane, M. A., & Lyon, B. (2014). The East African long rains in observations and models. *Journal of Climate*, *27*(19), 7185–7202. https://doi.org/10.1175/jcli-d-13-00447.1

Yang, W., Seager, R., Cane, M. A., & Lyon, B. (2015). The annual cycle of East African precipitation. *Journal of Climate*, *28*(6), 2385–2404. https://doi.org/10.1175/jcli-d-14-00484.1

Zscheischler, J., Orth, R., & Seneviratne, S. I. (2015). A submonthly database for detecting changes in vegetation-atmosphere coupling. *Geophysical Research Letters*, *42*, 9816–9824. https://doi.org/10.1002/2015GL066563

Zscheischler, J., & Seneviratne, S. I. (2017). Dependence of drivers affects risks associated with compound events. *Science Advances*, *3*(6), ARTN e1700263). https://doi.org/10.1126/sciadv.1700263